Geochemistry Geophysics Geosystems G3

Published by AGU and the Geochemical Society

Article
Volume 12, Number 12
17 December 2011
Q12005, doi:10.1029/2011GC003826
ISSN: 1525-2027

Time-dependent changes in volcanic inflation rate near Three Sisters, Oregon, revealed by InSAR

S. N. Riddick and D. A. Schmidt

Department of Geological Sciences, University of Oregon, Eugene, Oregon 97403, USA (snr22@cornell.edu)

[1] An extensive area near the Three Sisters volcanic center, Oregon, has been actively uplifting since 1996. In this study we use Interferometric Synthetic Aperture Radar (InSAR) to assess the Three Sisters uplift in time and space from 1992 through 2010. We present the first InSAR line-of-sight time series of the deformation, refine the onset of volcanic intrusive activity, assess the changes in deformation through time, and determine whether inflation is still occurring. We model InSAR data to determine the source geometry that best describes the uplift and create an inflation time series of the deformation. Our results reveal an intrusion, located at ~5–7 km depth with a cumulative volume of magma of ~5–7 × 10^7 m^3 as of fall 2010. The input of magma started gradually around the summer of 1996, increased significantly from 1998 to 2003, and then decreased in rate from 2004 through 2010. We present evidence that a swarm in 2004 was associated with the decrease in the source inflation rate.

Components: 9600 words, 6 figures, 1 table.

Keywords: InSAR; Oregon; Three Sisters; deformation; volcano.

Index Terms: 1240 Geodesy and Gravity: Satellite geodesy: results (6929, 7215, 7230, 7240); 8485 Volcanology: Remote sensing of volcanoes (4337).

Received 3 August 2011; **Revised** 24 October 2011; **Accepted** 26 October 2011; **Published** 17 December 2011.

Riddick, S. N., and D. A. Schmidt (2011), Time-dependent changes in volcanic inflation rate near Three Sisters, Oregon, revealed by InSAR, *Geochem. Geophys. Geosyst.*, *12*, Q12005, doi:10.1029/2011GC003826.

1. Introduction

[2] The Three Sisters volcanic center is one of the most active areas of the Cascade Range and one of the most densely populated vent areas in the world [*Hildreth*, 2007]. A wide spectrum of volcanic hazards, as well as newly discovered deformation in 2001, requires this area to be continually monitored [*Wicks et al.*, 2002]. We contribute to the monitoring effort by creating the first InSAR line-of-sight (LOS) time series of the Three Sisters inflation and by analyzing the changes in the volcanic source behavior from 1996 through 2010. By spatially and temporally inspecting the ground uplift, we hope to improve our understanding of the source, the hazards associated with this intrusive episode, and the potential for future activity in this region.

[3] The Three Sisters region is located in the High Cascades of central Oregon (Figure 1) and includes composite volcanoes, shields, and cinder cones. North Sister is a basaltic andesitic composite volcano on a broad shield base formed by long-lived effusive volcanism [*Taylor*, 1981; *Schmidt and Grunder*, 2011]. South Sister, Middle Sister, and Broken Top are younger composite basaltic andesitic to rhyolitic

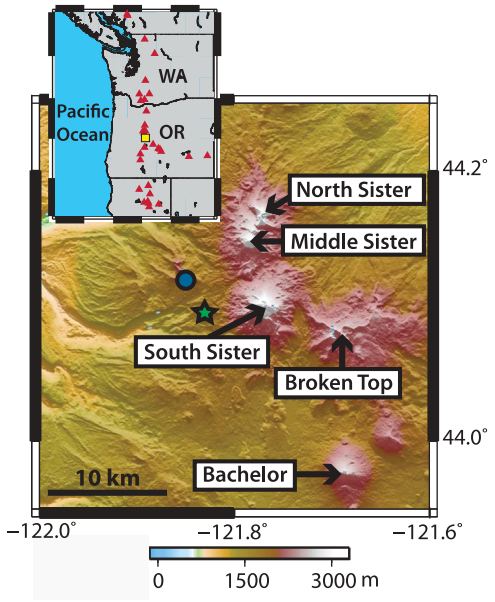

Figure 1. Area maps of the Three Sisters volcanoes. The Three Sisters volcanoes are located in central Oregon, shown by the yellow box in the inset. Red triangles represent locations of Cascade stratovolcanoes. A shaded relief map is shown with the Three Sisters, Broken Top, and Bachelor volcanoes indicated by arrows. HUSB is a continuous GPS station located at Husband indicated by the blue circle. The green star represents the approximate center of the uplifting area, ~5 km west of the summit of South Sister.

volcanoes with histories of explosive volcanism [*Taylor*, 1981; *Scott et al.*, 2001]. However, most of the volcanic activity in the Cascades is not related to the composite volcanoes. The majority (67–90%) of the volcanic activity in this area is associated with smaller mafic shields and cones that are distributed among the major composite volcanoes [*Sherrod and Smith*, 1990; *Hildreth*, 2007].

[4] The Three Sisters volcanic center has exhibited a range of eruptive activity within the past 2500 years. At approximately 2.2 and 2 ka, South Sister produced two rhyolitic flank eruptions of lava, pyroclastic flows, and tephra fallout with a combined total volume of about 0.85 km^3 [*Sherrod et al.*, 2004; *Hildreth*, 2007]. Between 2 and 1.5 ka, eruptions of basaltic to andesitic lava flows formed shield volcanoes and cinder cones near North Sister, including Belknap Crater, Four-in-One Cone, and Collier Cone [*Sherrod et al.*, 2004; *Hildreth*, 2007]. This geologically recent activity demonstrates that the region is still active and capable of producing comparable volcanic activity in the future. Potential volcanic hazards of the central Oregon Cascades include fallout of tephra, lava flows, pyroclastic flows, landslides from the steep volcano flanks, and lahars [*Scott et al.*, 2001]. The USGS has determined that due to the high level of activity and range of volcanic hazards, the Sisters region should be continually monitored [*Ewert et al.*, 2005].

[5] Prior to 2001, the Three Sisters volcanic field was thought to be dormant. However, *Wicks et al.* [2002] discovered a broad region of crustal uplift ~6 km west of South Sister. The area has been continuously uplifting since that discovery and monitoring efforts were last documented by *Dzurisin et al.* [2006, 2009]. No significant seismicity has been associated with the uplift except for a swarm of ~300 small magnitude earthquakes in March of 2004 located in the northeast section of the deforming area [*Moran*, 2004]. One deep long-period (DLP) earthquake was identified at ~12 km depth beneath the Three Sisters deforming area in 2006; DLPs are commonly associated with the presence of magma [*Nichols et al.*, 2011]. The potential cause of the Three Sisters deformation has been explored, including a magmatic source or the pressurization of a hydrothermal system [*Wicks et al.*, 2002; *Dzurisin et al.*, 2006, 2009]. *Wicks et al.* [2002] argue that the deformation is not caused by a hydrothermal system due to the lack of persistent or sporadic seismicity and lack of hot springs or thermal pools, all of which are commonly associated with geothermal systems. Furthermore, spring geochemistry provides evidence of a long-lived magmatic source at depth [*Ingebritsen et al.*, 1994; *Evans et al.*, 2004]. *Dzurisin et al.* [2009] conclude that the Three Sisters deformation can be attributed to an intrusion of magma at ~5 km depth.

[6] This paper expands the monitoring effort for the Three Sisters region by more fully documenting the time-dependent uplift related to the injection of magma at depth. We use InSAR data from 1992 through 2010 to create LOS time series and characterize changes in the volcanic source behavior in time. Utilizing persistent scatterer (PS) InSAR time series, small-baseline time series, and stacking, we refine the onset of the volcanic activity as well as determine whether the source is still inflating. By using an inflation time series, we are able to quantify the volume of magma injected into the crust and provide a more temporally complete timeline of the activity.

2. Data and Methods

2.1. InSAR

[7] We processed ERS, ENVISAT, and ALOS SAR data to image the deformation over the Three

Sisters area. We utilized ROI PAC software to process the SAR data and create interferograms [*Rosen et al.*, 2004], as well as the package SNAPHU to unwrap the interferograms [*Chen and Zebker*, 2002]. A 30-m resolution DEM produced from SRTM data covering the Three Sisters area was used to remove topographic contributions to the phase in interferogram processing [*Farr and Kobrick*, 2000]. Orbit files were used to estimate and remove the orbital error. Only ERS and ENVISAT interferograms with perpendicular baselines of 500 m or less were processed. Interferograms with baselines higher than ~500 m are normally too incoherent to detect deformation. Furthermore, only summer and early fall SAR scenes were considered in our analysis due to winter snow cover in the Cascades. Given these data constraints, we processed ~800 interferograms from seven ascending and six descending satellite tracks covering the Three Sisters area and analyzed these data with a variety of complementary methods.

[8] InSAR has been the main method to study the Three Sisters deformation because of its locality within a wilderness area. However, the dense vegetation and snow pose a great challenge to this method by causing decorrelation of the radar signal. Correlated areas of interferograms in the Three Sisters region are limited mainly to the sparsely vegetated lava flows. The degree of decorrelation is dependent on the wavelength of the radar signal used by the satellite. Since L-band data (~24 cm) has a longer wavelength than C-band data (~6 cm), L-band would be the best choice to obtain a more spatially complete deformation pattern. However, L-band data is less precise than C-band, making it more difficult to detect small signals [*Sandwell et al.*, 2008]. Additionally, L-band data from the ALOS satellite is only available after 2006. Unfortunately, the Three Sisters deformation rates from 2006 through 2010 are too small to be detected by L-band. Thus, our analysis focused on the C-band radar data acquired by the ERS and ENVISAT satellites operated by the European Space Agency (ESA).

[9] Decorrelation of C-band data, and inability to obtain information from ALOS L-band data, requires that other techniques must be used to obtain a more spatially complete deformation pattern. By using a variety of techniques such as StaMPS, single interferogram InSAR, stacks of interferograms, time series of small-baseline interferograms, and modeling, we examine the Three Sisters deformation in time and space to better characterize and quantify the magmatic inflation source beneath the Three Sisters area.

[10] We stacked interferograms of differing time intervals to obtain rates of deformation with reduced noise. Atmospheric artifacts resulting from the heterogeneous distribution of water vapor in the atmosphere are the greatest source of error in individual interferograms. To minimize this error source and resolve the deformation signal, we stacked sets of interferograms on each track [e.g., *Zebker et al.*, 1997; *Sandwell and Price*, 1998]. Although we processed data from thirteen satellite tracks, only seven of these tracks have at least five interferograms with sufficient coherence. Six of the seven tracks are ERS and ENVISAT, and thus data from only these tracks were modeled and analyzed in this study.

[11] An InSAR time series inversion developed by *Schmidt and Bürgmann* [2003] was also implemented to characterize the time-dependent signal. The method linearly inverts independent unwrapped interferograms for a LOS time series. Only the most coherent interferograms with little to no atmospheric or topographic errors were utilized. We used interferograms with perpendicular baselines of ~150 m or less to maximize coherence and minimize systematic topographic errors. We also imposed minimal temporal smoothing and averaged the range-change over a radius of 3 pixels. The small-baseline time series determines the amount of deformation in each epoch between SAR acquisition dates relative to a stable area far from the deformation.

[12] Finally, we implemented StaMPS version 3.2b3 to study the Three Sisters deformation using the persistent scatterer method [e.g., *Hooper et al.*, 2007; *Hooper*, 2008]. StaMPS is an algorithm that identifies surface scatterers (buildings, rock outcrops, etc.) with stable radar characteristics that are called persistent scatterers. The phase is selected only on those points, which allows the deformation signal to be recovered from some areas that were decorrelated in single interferograms. The final output of StaMPS is a time series showing cumulative deformation. The time series results from StaMPS were compared directly with the small-baseline time series discussed in the previous paragraph. We used default parameters during StaMPS processing and analyzed the unwrapped phase with the DEM, orbit, and atmospheric error removed.

2.2. Modeling

[13] To better characterize the magmatic source, we modeled our InSAR observations using a Mogi model, tension crack model, and ellipsoid model to determine the best fit to the Three Sisters

deformation and better understand the magmatic source. The most basic and commonly used magmatic inflation model is the Mogi model, a point pressure source in an elastic half-space [*Mogi*, 1958]. We also implemented a tension crack model to determine the best fit for a dike or sill-like source [*Yang and Davis*, 1986]. Preliminary modeling showed that a vertical dike would not fit the data, and so we did not pursue a dike any further. The horizontal crack model was used as an approximation of a sill. The ellipsoid model was an approximation of a vertical spheroidal source [*Davis*, 1986].

[14] We modeled separate stacks of interferograms for each satellite track and solved for tilts and offsets that may have been caused by orbital ramps that were not successfully removed during interferogram processing. Due to significant topography in the Three Sisters region, the models included a topographic correction to account for how the topography affected the deformation signal in regions of high relief [*Williams and Wadge*, 2000]. Green's functions that relate the surface deformation to the inflation of a buried source in an elastic half-space [*Mogi*, 1958; *Yang and Davis*, 1986; *Davis*, 1986] were calculated using *Williams and Wadge*'s [2000] package, Topodef. Deformation models for an inflation source showed a tradeoff between volume change and depth. Thus, we iteratively inverted the LOS observations for the volume change rate while varying the depth. Furthermore, for the ellipsoidal source, the ratios of the three axes were solved for and we iterated for depth using the best fit axis ratios for each track. Jackknifing of the stacks was also implemented to determine the sensitivity of the model to data variability [e.g., *Miller*, 1974]. For the jackknifing, one interferogram was taken out from each stack at a time and the inversion was rerun iteratively.

2.3. Source Inflation Time Series

[15] While the small-baseline time series provides a record of the surface deformation from individual satellite tracks, we also produced a time series of the inflation source utilizing all of the high quality interferograms on varying tracks in a combined inversion. ERS data provide yearly SAR acquisitions from 1992 through 2008 with multiple year gaps of no useable data due to gyroscope malfunctions of the satellite. ENVISAT SAR data only span 2003 through the present. Because each satellite and track's data have different SAR acquisition dates, and only summer and fall data can be used, time series for each track are irregularly sampled in time. Combining the two satellites' data from all tracks fills in the data gaps and provides the most temporally complete time series. To do this, the data of different look angles must be related to a look angle independent term such as pressure or volume change of an inflation source. We related the best single interferograms, i.e., those interferograms with good coherence, small perpendicular baselines, and minimal atmospheric artifacts, to the volume change of the best fit source model. Using the least squares formulation of *Grandin et al.* [2010] with the optimal source depth from our modeling, we inverted for the source inflation time series. We calculated the uncertainty of the inflation time series by propagating the observational error through the inversion using a standard least squares approach. The spatially correlated error of the interferograms was defined by constructing a data covariance assuming a 5 mm standard deviation for neighboring pixels with a spatial correlation that decays over 10 km [*Lohman and Simons*, 2005]. The inflation time series presents cumulative volume for each SAR acquisition epoch from 1992 to 2010.

3. InSAR Results

[16] The observed deformation in our interferograms is a broad ~20 km-by-30 km area with the north–south extent spanning from ~5 km south of Belknap Crater to the latitude of Mount Bachelor, and the east–west extent ranging from Broken Top to ~15 km west of the peak of South Sister (Figure 2). The center of maximum uplift is located approximately ~5 km west of the peak of South Sister. The SAR satellites record an increase in the LOS range-change, which corresponds to uplift of the ground if all deformation is assumed to be vertical. The deformation pattern is not perfectly symmetrical, with a slight extension of the signal along an axis rotated about 10–20 degrees clockwise from north. The coherence is good in the summer and fall for the High Cascades where there is less vegetation, but coherence decreases rapidly over the densely forested Western Cascades.

[17] The InSAR time series help to image the time-dependent evolution of the deformation. The small-baseline time series reveals a gradual start to the deformation of ~1 cm/yr, which then increases to a maximum uplift rate of 3–4 cm/yr from 1998 through 2003 (Figure 3). After the summer of 2003, the deformation rate decreases. StaMPS time series confirm these results with similar trends in the LOS range-change. The total amount of LOS

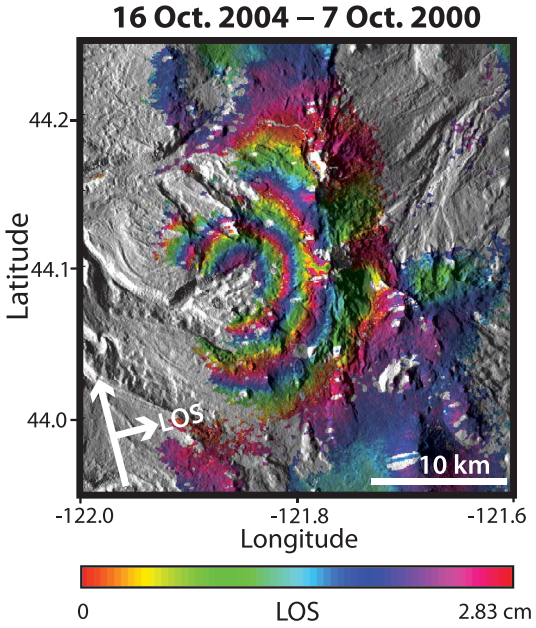

Figure 2. An exemplary interferogram showing as much as 8 cm of line-of-sight (LOS) surface deformation along Track 163 of the ERS satellite. The convention used in this paper is positive LOS corresponds to a decrease in distance between the satellite and ground. The interferogram covers a nearly 4-year period from 7 October 2000 to 16 October 2004. Arrows indicate the LOS look direction (to the ENE) and the flight path of the satellite (to the NW). The interferogram is overlaid on a shaded relief image of the same region shown in Figure 1.

range-change from the onset through 2010 is approximately 25 cm. The 2010 LOS rate is small, on the order of several millimeters to one centimeter per year. Single interferograms did not show a clear signal, but all three ENVISAT stacks show average peak LOS rates of ~6–8 mm/yr from 2006 to 2010. There is also good agreement between the small-baseline time series and a GPS time series for the station HUSB (Figure 3; see Figure 1 for the location of HUSB). The GPS time series also suggests a small amount of deformation occurring in 2010.

4. Modeling Results

4.1. Modeling of InSAR Stacks

[18] The deformation resolved by InSAR is indicative of a pressurized magma source at depth. As a first-order exploration of the inflation source, a Mogi model was considered due to the relatively symmetrical shape of the ground deformation [*Mogi*, 1958]. Using the InSAR stacks, we iteratively invert for the optimal volumetric inflation rate while varying the source depth. The Mogi model gives source depths ranging from 4 to 5.5 km with volume change rates of $2–4 \times 10^{-3}$ km^3/yr (Table 1). The model fits the data extremely well based on the residuals (Figures 4a–4c and Table 1). The ranges of values in the tables signify model sensitivity to data variability from jackknifing of the stacks. Not surprisingly, the tracks with the least number of interferograms in the stacks have greater variability in depth and/or volume change rates.

[19] We also implemented a tension crack model to determine if the source could be described as a sill (Figures 4d and 4e). The horizontal crack model gives depths deeper than the Mogi model, ranging from 6 to 8 km but with slightly smaller volume change rates of $1–3 \times 10^{-3}$ km^3/yr (Table 1). Additional modeling details concerning the crack model can be found in Appendix A.

[20] Model results of a triaxial ellipsoid point source model [*Davis*, 1986] are similar to those of the Mogi and crack models (Figures 4f and 4g). The

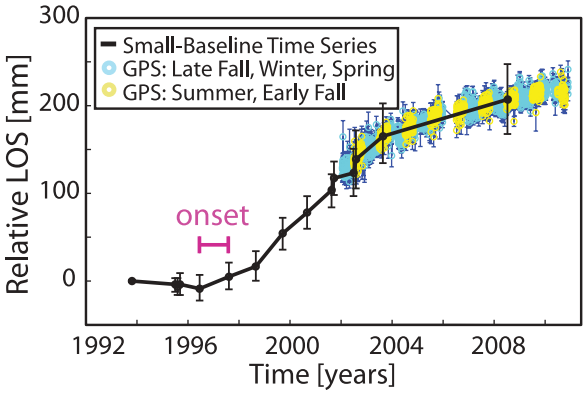

Figure 3. A small-baseline time series of T385 ERS interferograms (black) and GPS time series (blue and yellow). The small-baseline time series represents an average of neighboring pixels centered over the area of greatest range-change. Positive LOS range-change starts gradually after 30 June 1996 with the rate increasing through 2003. Black error bars represent +/− 1 sigma uncertainties. These were estimated by propagating a LOS error of 5 mm through the small-baseline time series inversion. Continuous GPS data for station HUSB is available after 2002 (Figure 1; denoted by blue circle). The vertical, north, and east components are projected onto the line-of-sight for T385 ERS. Yellow colored circles correspond to the summer and fall for a direct comparison to InSAR; Cyan circles represent snow covered months. Dark blue error bars are calculated based on the error of all three GPS components. GPS data and errors were obtained from the Pacific Northwest network on the USGS website.

Table 1. Mogi, Tension Crack, and Ellipsoid Model Results[a]

Mogi Model Results				
Track	Volume Δ Rate (km^3/yr)	Depth (m)	RMSE ($\times 10^{-4}$ m)	Date Range
113 ERS (30)	0.0020 [$+2.0 \times 10^{-4}$, -0.40×10^{-4}]	4000 [+200, −100]	7.3 [+0.3, −0.8]	06/1992–09/2003
113 ENVI (16)	0.0017 [$+2.2 \times 10^{-4}$, -1.7×10^{-4}]	4800 [+500, −400]	8.7 [+0.9, −0.5]	07/2003–09/2010
385 ERS (37)	0.0038 [$+1.3 \times 10^{-4}$, -2.4×10^{-4}]	5200 [+100, −100]	6.3 [+0.2, −0.1]	08/1993–08/2008
385 ENVI (16)	0.0019 [$+4.2 \times 10^{-4}$, -2.6×10^{-4}]	5500 [+700, −400]	6.2 [+0.5, −0.2]	06/2003–09/2010
163 ERS (5)	0.0025 [$+2.1 \times 10^{-4}$, -4.6×10^{-4}]	4500 [+300, −300]	9.1 [+3.6, −0.0]	08/1995–10/2004
163 ENVI (9)	0.0018 [$+2.4 \times 10^{-4}$, -2.3×10^{-4}]	4600 [+500, −400]	10.0 [+1.3, −0.3]	09/2004–09/2010
Crack Model Results				
Track	Volume Δ Rate (km^3/yr)	Depth (m)	RMSE ($\times 10^{-4}$ m)	Length (m)
113 ERS	0.0017 [$+1.5 \times 10^{-4}$, -0.30×10^{-4}]	6000 [+300, −200]	7.2 [+0.3, −0.9]	2700 [+100, −0]
113 ENVI	0.0014 [$+1.6 \times 10^{-4}$, -1.4×10^{-4}]	7000 [+500, −500]	8.8 [+0.9, −0.5]	2200 [+100, −100]
385 ERS	0.0032 [$+10 \times 10^{-4}$, -1.9×10^{-4}]	7600 [+100, −100]	6.0 [+0.3, −0.1]	3600 [+0, −100]
385 ENVI	0.0016 [$+3.3 \times 10^{-4}$, -2.0×10^{-4}]	7800 [+800, −500]	6.3 [+0.5, −0.2]	2300 [+100, −100]
163 ERS	0.0021 [$+2.9 \times 10^{-4}$, -2.9×10^{-4}]	6600 [+300, −500]	10.5 [+2.1, −0.6]	2700 [+100, −100]
163 ENVI	0.0017 [$+1.9 \times 10^{-4}$, -1.9×10^{-4}]	7000 [+600, −600]	9.9 [+1.3, −0.8]	2200 [+100, −100]
Ellipsoid Model Results				
Track	Volume Δ Rate (km^3/yr)	Depth (m)	RMSE ($\times 10^{-4}$ m)	Axis Ratios (b:a, c:a)
113 ERS	0.0014 [$+1.3 \times 10^{-4}$, -0.20×10^{-4}]	5100 [+300, −200]	7.1 [+0.4, −0.9]	0.6:1, 0.4:1
113 ENVI	0.0012 [$+1.6 \times 10^{-4}$, -1.2×10^{-4}]	5200 [+400, −500]	8.4 [+0.8, −0.4]	0.1:1, 0.1:1
385 ERS	0.0029 [$+1.0 \times 10^{-4}$, -1.7×10^{-4}]	6300 [+100, −100]	6.0 [+0.3, −0.1]	0.5:1, 0.4:1
385 ENVI	0.0015 [$+3.1 \times 10^{-4}$, -1.9×10^{-4}]	6600 [+800, −500]	6.0 [+0.5, −0.1]	0.5:1, 0.4:1
163 ERS	0.0016 [$+2.1 \times 10^{-4}$, -2.2×10^{-4}]	6100 [+300, −1000]	10.1 [+1.9, −0.8]	0.3:1, 0.2:1
163 ENVI	0.0015 [$+1.9 \times 10^{-4}$, -1.8×10^{-4}]	6300 [+600, −500]	9.8 [+0.1, −0.8]	0.4:1, 0.3:1

[a]Parentheses indicate the number of interferograms used for each track. The value ranges in brackets are from jackknifing. RMSE is the Root Mean Square Error. The Date Range column gives the time spanned by each track's stack, and applies to all models.

best fit depth ranges from 5 to 6.5 km with volume change rates of 1–3 $\times 10^{-3}$ km^3/yr (Table 1). The inversion solved for the source axis ratios, which allowed for a better fit to the data by accounting for the slight asymmetry in the deformation. Although the RMSE for the ellipsoid model are generally lower, they are not significantly lower given the extra modeling parameters and thus not able to discriminate the ellipsoidal model as better than the other models. The variability in volume change rate among satellite tracks is largely due to the different years spanned by each track's stack. An inflation time series is needed to resolve the variable volume change in time.

4.2. Source Inflation Time Series

[21] To better constrain the time-dependent inflation of a volcanic source, we inverted for an inflation time series using all the best quality interferograms on four different tracks. We performed the inflation time series for the Mogi, crack, and ellipsoid models. However, in this section, we focus on implementing the inflation time series for the crack model. Reasoning for this preference is examined in section 5.2. The depth of the source was assumed fixed at 7 km, which was the average crack depth of the six modeled tracks. Green's functions were calculated that relate the source inflation rate for a buried horizontal crack to the LOS deformation rate observed along each satellite track. The resulting inflation time series shows a relatively steady increase in volume after the summer of 1996 and then increases almost linearly from 1998 through 2003 at 7.8 $\times 10^6$ m^3/yr. A change in the slope of the time series occurs around 2004, to a more modest rate of 1.6 $\times 10^6$ m^3/yr (Figure 5). The shape of the inflation curve closely matches the LOS time series as expected (Figure 3).

[22] The change in inflation rate from before and after 2004 is supported by leveling data presented by *Dzurisin et al.* [2009]. Yearly August leveling surveys revealed that uplift rates from 2002 to 2004 were ~50% higher than from 2004 to 2006, suggesting a possible relationship between the seismicity and inflation. Whereas *Dzurisin et al.* [2009] favored an exponential decay of the deformation from 1998 to 2006, our longer time series, with data through 2010, more clearly shows that there are two

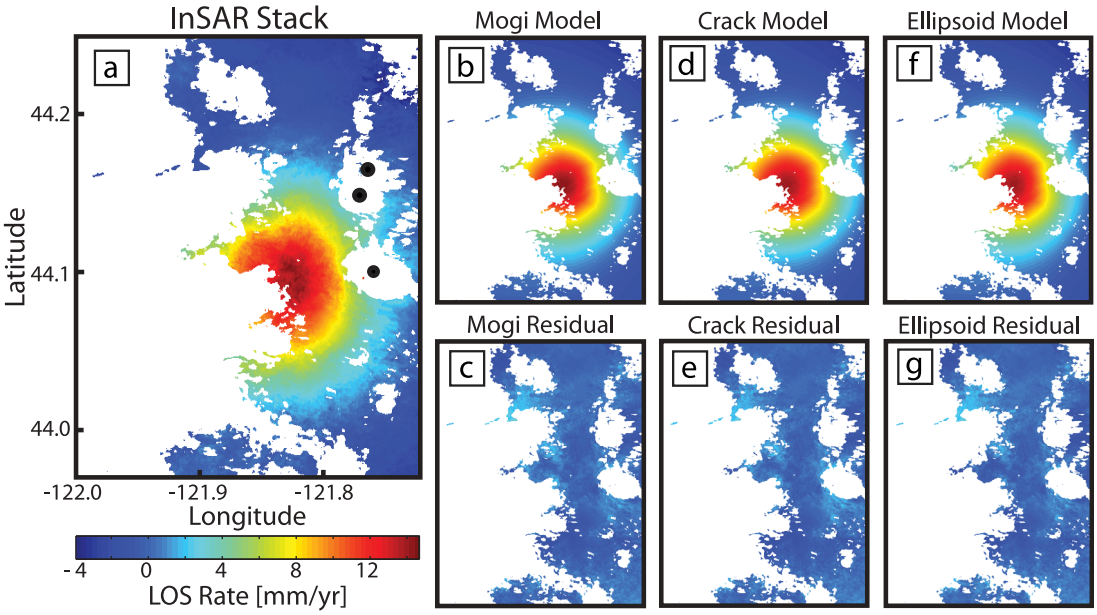

Figure 4. Data and model results for T385 ERS. (a) LOS rate for T385 ERS stack used in modeling. The stack is made from 37 interferograms spanning 26 August 1993 through 31 August 2008. Black dots represent the locations of the Three Sisters volcanoes for reference. (b) The predicted Mogi model. (c) The residuals from the data minus the Mogi model (Figures 4a and 4b). (d) The predicted tension crack model. (e) The residuals from the data minus the tension crack model (Figures 4a and 4d). (f) The predicted ellipsoid model. (g) The residuals from the data minus the ellipsoidal model (Figures 4a and 4f). The parameters used to make the above models (Figures 4b, 4d, and 4f) are in Table 1 for the T385 ERS stack row.

trends after 1998, with the change in slope corresponding to about the time of the March 2004 seismic swarm. The RMSE for the two linear trends (summer 1998 – fall 2003 and summer 2004 – fall 2010) is 28% lower than that of an exponential fit. A one-tailed F test reveals that at the 5% significance level, we can reject the null hypothesis that an exponential model and two linear trends model can describe the data equally well. This statistical analysis of the inflation time series provides evidence of a change in the intrusion behavior at about the time of the swarm.

[23] Furthermore, our inflation time series indicates that the cumulative volume of the sill-like intrusion

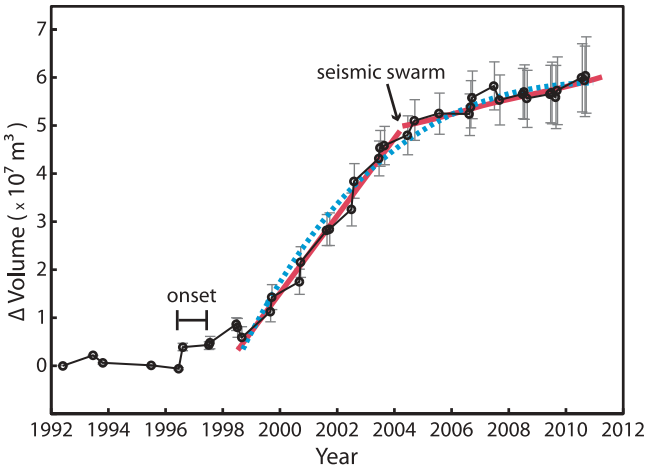

Figure 5. An inflation time series (black circles) for a sill-like source combining 56 interferograms from four ERS and ENVISAT tracks. Gray error bars are +/− one standard deviation. The red lines indicate two linear trends, from 1998 to 2004 and 2004 to 2010 with slopes of 7.8×10^6 m^3/yr and 1.6×10^6 m^3/yr, respectively. The dashed blue line is the best fit exponential curve, which does not fit the time series as well as the two linear trends.

as of late 2010 is 6.05×10^7 m^3 (Mogi source: 7.02×10^7 m^3; Ellipsoid source: 4.92×10^7 m^3). This value is the same order of magnitude of that projected by *Dzurisin et al.* [2009], who estimated that the entire episode will have a total volume of ~4.5 to 5×10^7 m^3. An intrusion of this size is relatively small, common and comparable in magnitude to other intrusive source volumes, such as that observed in the Aleutians [e.g., *Lu et al.*, 2002, 2003]. *Dzurisin et al.* [2009] provide a more comprehensive discussion of how the Three Sisters inflation compares to other volcanic systems.

5. Discussion

5.1. Onset of Deformation

[24] An important goal in our study is to precisely determine the timing and abruptness of the onset of deformation. We interpret an abrupt onset to be newly (re)activated volcanic activity that reaches its maximum inflation rate (or erupts) within hours to months of onset. In contrast, we define a gradual onset as activity that takes years to decades to reach the maximum inflation rate or an eruptive event. Many newly activated volcanoes exhibit a sudden onset, such as the recent 2004 eruption of Mt. St. Helens, which displayed intense seismicity, localized surface deformation, and explosions within the first three weeks [*Scott et al.*, 2008]. Similarly, Chaitén volcano had a rapid onset, erupting explosively within two days of seismic activity, and exhibiting no observable surface deformation two weeks prior to the eruption [e.g., *Fournier et al.*, 2010, and references therein; *Wicks et al.*, 2011, and references therein]. However, other volcanic systems, including the Three Sisters, are not as clear as to whether the onset is abrupt or gradual, with no indication of activity other than surface deformation detected by InSAR, GPS, or leveling surveys. For our study area, InSAR is the only data set that spans the onset, and can characterize the timing and character of the new activity. By analyzing InSAR time series and stacking, we determined that the deformation did not have a sudden onset like St. Helens or Chaitén, but instead had a gradual onset with a lower LOS rate (~1 cm/yr) in the first couple of years followed by the higher 3+ cm/yr rate from 1998 to 2003. Volcanic systems exhibiting gradual onsets are rarely discussed in the volcanic literature. However, we hypothesize that many other active, aseismic volcanic systems exhibit gradual onsets, but due to temporal gaps in data and/or lack of geodetic networks, are never fully resolved.

[25] Aseismic volcanic activity poses a great risk, because a large volume of magma can accumulate over several years and culminate in an eruption with little warning. With the Three Sisters area, magma had accumulated at depth for five years before the volcanic activity was detected. Fortunately, this system has yet to erupt, but other intrusive episodes might not be as long-lived before an eruption. Geodetic methods such as GPS and tiltmeters would be best at quickly detecting onsets. However, if the onset is missed by these methods, or these networks do not exist in the region of activity, we believe that InSAR stacking and time series are the most viable methods to quickly detect small aseismic deformation events.

[26] Previous publications on the Three Sisters deformation proposed varying onsets from the summer of 1996 through the fall of 2000 [*Wicks et al.*, 2002; *Dzurisin et al.*, 2006, 2009]. Because such a range of start times exist, we analyzed the InSAR data in detail with single interferograms, stacks, small-baseline time series, and StaMPS time series to arrive at a precise time of onset derived solely from InSAR. Single interferograms did not provide an exact onset date because most were completely incoherent or had artifacts that made interpretation inconclusive. This explains why previous researchers could not give a definitive or more specific time for the onset based on the interferograms. Thus, other methods are needed to help refine the initiation of deformation.

[27] The inception of deformation was further assessed from our InSAR time series. We inspected the individual epochs of StaMPS results for T385 ERS (Figure 6a) which revealed no uplift occurring in the June 1996 epoch (Figure 6b) but uplift transpiring in the July 1997 epoch (Figure 6c). Both epochs were referenced to the first date shown in Figure 6a. Because the June 1996 image showed no deformation, this implies that the deformation in the July 1997 image must have occurred between 30 June 1996 and 20 July 1997. The small-baseline inversion for T385 ERS data confirms that the deformation began between 30 June 1996 and 20 July 1997 (Figure 3). Similarly, this is seen in StaMPS T113 ERS, which reveals that deformation started between 20 August 1996 and 5 August 1997. Using information from both tracks implies an onset of deformation between 20 August 1996 and 20 July 1997. To provide further verification we used InSAR stacks to find a small signal that was spatially consistent through time. Stacking different subsets of interferograms revealed no deformation from 1992 to 1995, a small amount of deformation

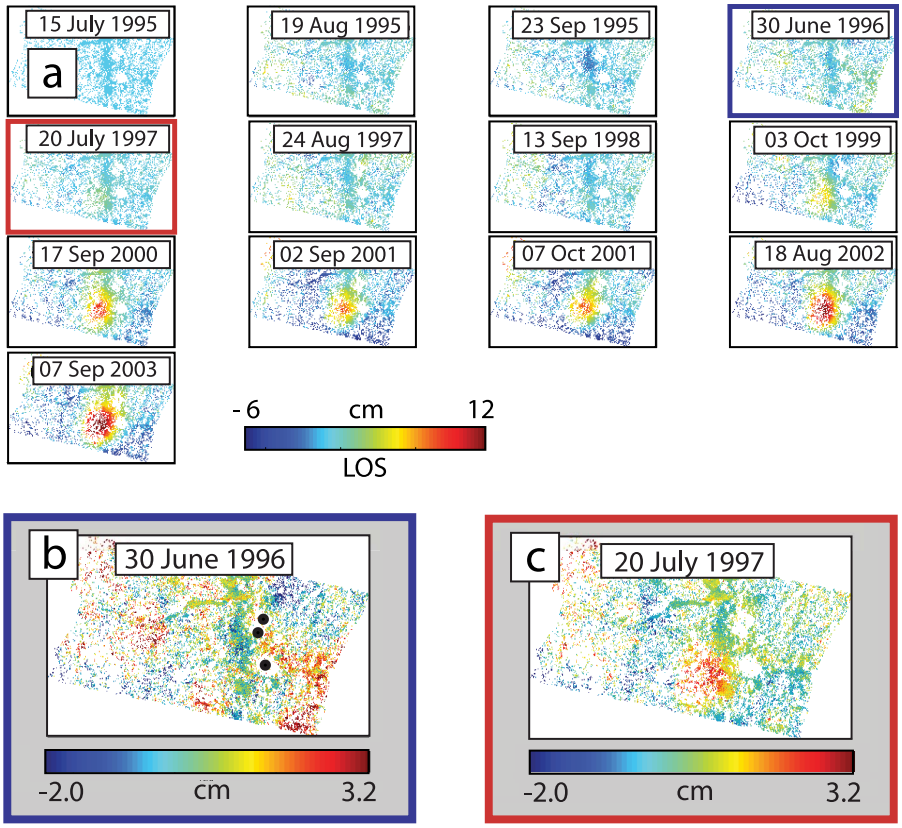

Figure 6. StaMPS results for T385 ERS. Each image shows cumulative LOS range-change with reference to the first scene of 15 July 1995. The region shown in each frame is roughly similar to Figure 1. (a) Cumulative LOS range-change from 15 July 1995 to 07 September 2004. The blue and red boxes correspond to Figure 6b and Figure 6c, respectively. (b) Blue box in Figure 6a with a smaller scale to detect a small signal. This image shows that there is no deformation over the uplift area from 15 July 1995 to 30 June 1996. Black dots represent the approximate locations of the Three Sisters volcanoes for reference. (c) Red box in Figure 6a with the same scale as Figure 6b. This image shows the cumulative deformation from 15 July 1995 to 20 July 1997 with a circular uplift pattern west of South Sister. Since Figure 6b shows that no deformation occurred through 30 June 1996, this implies that the uplift must have started between 30 June 1996 and 20 July 1997.

between July 1995 to August 1997, and significant deformation after August 1997. We conclude using time series and stacking that the onset began between the summer of 1996 and summer 1997, and started gradually by exhibiting a lower rate over several years in comparison to the high rate after 1998. Although the SAR acquisitions and the seasonal effects of snow limit the time of onset given here, it is as tightly constrained as possible with InSAR. If the area of study was in a locality with little to no snow, the onset of deformation could be narrowed to within a few months.

5.2. Volcanological Interpretation

[28] The Three Sisters deformation source geometry is non-unique based on the results of the three source models implemented in this study. This is partly due to the near symmetrical shape of the deformation pattern, which can be described by all three models, and the fact that deeper sources are poorly resolved. Since surface deformation data is unable to distinguish the source geometry, spherical, sill-like, and ellipsoidal source geometries are all possible. However, several geologic considerations suggest the source of the deformation is most likely to be a sill. The Mogi model is an idealized point source and the geometry of the source is also not likely to be perfectly spherical. Moreover, magma chambers of any shape, whether spherical or ellipsoidal, are now recognized as uncommon [*Gudmundsson*, 1990; *Menand*, 2011]. This is because of the special and limited conditions required to develop and maintain a magma chamber. An active magma chamber requires a delicate balance of heat in and out of the system so that a large

portion of the magma reservoir can be erupted. Numerical simulations also show that active magma chambers can only develop with a limited range of emplacement rates [*Annen*, 2009]. In contrast, single or repeated intrusions of sills are frequent, and there is a wealth of field evidence documenting these structures [*Menand*, 2011]. Furthermore, sills are already known to be frequent in the Three Sisters area. Erosion of the edifice has exposed hundreds of dikes and sills near North Sister [*Williams*, 1944; *Hildreth*, 2007]. Broken Top also has many mafic dikes and sills intruding its cone [*Hildreth*, 2007].

[29] In addition to the geologic predominance of sills, the lack of seismicity associated with the inflation is consistent with the deeper source depth found for the sill model. For the deformation to be aseismic, the source would need to be deep enough to be at or near the brittle-ductile transition, which is thought to be as shallow as 5 km depth beneath active volcanoes [*Hill*, 1992]. Brittle-ductile transition zones beneath volcanoes have also been shown to be deeper, between ~6–9 km [e.g., *Bryan et al.*, 1999; *Soosalu et al.*, 2010; *White et al.*, 2011]. Our Mogi model results are shallower than ~5.5 km and the ellipsoidal results extend to ~6.5 km. If magma was injected to this shallow level, we would have expected greater seismicity in the region during the intrusion. The sill depths for each track are deeper than the other model results, with an average of 7 km.

[30] Several petrological studies of the Cascades provide evidence of magma storage at or around 7 km depth, the average of our sill model results. Data from melt inclusions collected at Collier Cone and Four-in-One Cone near North Sister give mid to upper-crustal magma storage depths. Melt inclusions of the cinder cones near North Sister suggest that magma is commonly stored at 100–200 MPa [*Ruscitto et al.*, 2010], which corresponds to depths of ~4–8 km. However, these results are considered minima due to CO_2-rich vapor bubbles within the melt inclusions, and likely the storage depth would be toward the upper range of 6–8 km or deeper (D. M. Ruscitto, personal communication, 2011). These results favor the deeper depths given by the sill model and also provide verification that the model results agree with the geochemistry of the Three Sisters area. Furthermore, this equilibration depth is similar to that found elsewhere in the Cascades, such as at Mount St. Helens where data indicate a source depth of at least 7 km for material erupted in May 1980 [e.g., *Rutherford et al.*, 1985; *Pallister et al.*, 1992]. Two earthquake studies propose a magma source region between 7 and 14 km and 6.5–10 km beneath Mt. St. Helens [*Scandone and Malone*, 1985; *Moran*, 1994]. This may imply a common preferential depth for a brittle-ductile transition zone beneath Cascade volcanoes at about 7–10 km depth.

[31] The injection of magma into the crust that does not culminate in an eruption is common in volcanic arcs. This is evidenced by the geologic record and by intrusive/extrusive ratios, which indicate that volumes of intrusive rocks are much higher than extrusive rocks and that intrusions are more common than eruptions [e.g., *White et al.*, 2006, and references therein]. The periodic long-term emplacement of magma is likely part of the volcanic cycle and vital for recharging volcanic systems. *Dzurisin et al.* [2006] speculate that intrusive episodes last from days to years and are separated by quiescent periods of tens-to-hundreds of years. Melt at depth is fed to a mid to upper-crustal storage region via dikes in episodic surges. If these intrusions of magma are closely spaced in time, this can keep the previous pulse of melt from solidifying and allow for magma to accumulate. When enough magma has accumulated through several intrusions, a threshold is reached and an eruption could take place. With this continued process in mind, the Three Sisters area should be continually monitored, especially if this intrusion continues or if another intrusion occurs within several years of this episode. Geochemical evidence from springs of the Three Sisters area indicates that this intrusive episode is likely the latest in a series of magma intrusions [e.g., *Ingebritsen et al.*, 1994; *Wicks et al.*, 2002; *Evans et al.*, 2004]. These intrusions could be forming or adding to an extensive intrusive complex. Likely, intrusions such as these occur frequently in the Cascades but can elude detection due to their aseismic nature.

[32] The ongoing deformation is clearly offset from the Three Sisters stratovolcanoes, and if the inflation source erupted, it would likely produce a new cinder cone. A cone is likely because most eruptive activity in the central Oregon Cascades forms mafic shields and cones [*Hildreth*, 2007], and the amount of magma we calculated for this intrusive episode represents a relatively minor pulse. *Hildreth* [2007] also comments that nowhere else in the Cascades are vent alignments more evident than in this region, where lines of mafic volcanoes and chains of rhyolitic vents form many north-trending arrays. It is plausible that the current deformation sits above a zone of weakness within the high Cascades

and that these north–south zones of weakness are likely responsible for many of the cinder cone chains in the region.

[33] Although we conclude that the deformation near the Three Sisters volcanoes is most likely due to a single tabular basaltic sill, realistically it may be much more complex. The recent intrusion probably adds to a pre-existing extensive intrusive complex and it is unclear whether the successive intrusions could culminate in an eruption or instead form a laccolith or lopolith by the amalgamation of magma injections.

[34] The one swarm of ~300 small magnitude earthquakes in late March of 2004 was likely due to stress build up in the upper crust from the continual inflation over ~8 years, or from volatiles rising off of the intrusion. The crust relieved some of the accumulated stress by means of the earthquake swarm along favorably oriented faults adjacent to the source center. Interestingly, the seismic swarm may be related to the distinct change of slope in the inflation time series in 2004. This is the first known evidence for a possible connection between the deformation and the seismicity in the Three Sisters area.

6. Conclusions

[35] We use single interferograms, stacks, LOS time series, inflation time series, and modeling to examine deformation near the Three Sisters volcanoes of Oregon. We interpret the deformation to be caused by the intrusion of magma at depth, resulting in ~25 cm of uplift through 2010. The uplift began gradually between late summer of 1996 and summer of 1997, and then increased to ~3–4 cm/yr from 1998 through 2003. A marked decrease to ~20% of the peak uplift rate occurred in 2004 and continues through 2010. This change in intrusion behavior may be related to the seismic swarm that occurred in late March of 2004. In 2010, the uplift rate is near the magnitude of the noise, but appears to be holding constant at about 6–8 mm/yr.

[36] We explored the source of the deformation by modeling the InSAR data assuming a Mogi point source, a tension crack, and an ellipsoidal pressure source. All models describe the deformation equally well based on the fit to the data, and consequently we cannot resolve whether the source shape is spherical, sill-like, or ellipsoidal. But considering geophysical constraints and field data, we hypothesize that the source is most likely a sill of basalt at a depth of 7 km. The sill model gives deeper source depths than the Mogi and ellipsoid models. A deeper source is more probable due to the lack of seismicity from the inflation and because melt inclusion information from nearby cinder cones give a deep source depth. The total volume of magma intruded as of 2010 for a sill-like source is ~6×10^7 m^3, which is comparable in size to other modeled sills and other intrusions in the Aleutians. The Three Sisters area should be continually monitored because of the ongoing intrusion and the likelihood of future intrusive episodes. The duration, volume, and repeat time of these intrusive episodes are important for determining the potential volume of magma stored at depth as well as its likelihood of erupting.

Appendix A: Modeling Details

[37] Certain model parameters were fixed to reduce the complexity of the iterative inversion scheme. For the crack model, an aspect ratio of length/thickness of the sill was selected as 1000, and the width of the sill was assumed to be the same as the length due to the symmetry of the deformation signal. An aspect ratio of 1000 is a compromise between field data, experimental data, and inverse modeling. Studies that invert for sill dimensions (length or opening) from deformation data typically favor extreme maximum or minimum dimensions with very large aspect ratios of up to 2×10^6 [e.g., *Pedersen and Sigmundsson*, 2004]. However, many of these same studies also state that smaller lengths and larger openings can equally fit the data such that the total volume change is conserved. In contrast to the literature on inverse modeling, experimental and field data suggest that aspect ratios only range from <10 to 1000 [e.g., *Valentine and Krogh*, 2006; *Galland et al.*, 2007; *Menand and Phillips*, 2007; *Hansen et al.*, 2011]. The aspect ratio chosen in this study is a compromise between field data and that found from the modeling of geodetic data. Furthermore, higher aspect ratios correspond to lower viscosity composition magma, such as basalt, emplaced at several kilometers depth within the crust. It is likely that an intrusion near the Three Sisters would be basaltic to basaltic andesite, and thus would correspond to the aspect ratios on the higher end of the experimental and field observations. By fixing the aspect ratio, we reduced the number of free parameters in the model and thereby keep the analysis time of the iterative inversion scheme to a reasonable level. With the total volume of magma given by the inflation time series, we calculated the size of the

sill-like source. Assuming the length and width of the crack are equal, and that the aspect ratio of length to opening is 1000, we calculated the length and width to be ~3.9 km with a corresponding opening of 3.9 m.

[38] Both the Mogi and crack models describe the deformation equally well. However, the crack model has more degrees of freedom (dip, strike, etc.), many of which were fixed at the beginning. If these parameters had been optimized, the RMSE would likely be further reduced for the crack model. Because the RMSE were slightly lower for the ellipsoid model that solved for axis ratios, the assumption used in the crack model of an equal length and width is likely not sufficient. If the length and width were not assumed to be equal in the crack model, we would expect the RMSE to be similar to the ellipsoid model.

[39] Iterations for aspect ratio, strike and dip were explored for one track to determine the optimal ranges of these previously fixed parameters. The best fit aspect ratios are low, with the deformation best described by ratios of 5 to 4500. An aspect ratio of 5 gave the lowest RMSE, while an aspect ratio of 4500 gave a RMSE value of only 5% higher. The dip with the lowest RMSE is 6 degrees +/−6 degrees, and a southeast strike of 116 +/− 67 degrees clockwise from north. Uncertainties denote ranges where the RMSE varies by +/−5%. The strike is highly variable within a small RMSE range due to the shallow dip; in contrast, steeper dip angles would have tighter ranges due to significant reliance on strike for best fit.

[40] While we focused solely on elastic models to explain the deformation, viscoelastic models are an alternative approach. However, our time series suggest two linear trends indicative of a step change in the inflation rate, whereas an exponential decay in the deformation rate might be a hallmark of a viscoelastic response [*Newman et al.*, 2001]. While we cannot rule out some viscoelastic behavior, an elastic rheology allows us to more efficiently model the first-order characteristics of the deformation. Furthermore, these first-order approximations from elastic modeling are used in viscoelastic modeling to limit the free parameters, as geometrically parameterizing FEMs is time-intensive [e.g., *Newman et al.*, 2006].

Acknowledgments

[41] We would like to thank Chuck Wicks for providing ENVISAT data. Additional ENVISAT and ERS data were acquired through WInSAR from the European Space Agency. ALOS data were acquired by the Japanese Space Agency and obtained through the Alaska SAR Facility.

References

Annen, C. (2009), From plutons to magma chambers: Thermal constraints on the accumulation of eruptible silicic magma in the upper crust, *Earth Planet. Sci. Lett.*, *284*, 409–416, doi:10.1016/j.epsl.2009.05.006.

Bryan, C. J., S. Sherburn, H. M. Bibby, S. C. Bannister, and A. W. Hurst (1999), Shallow seismicity of the central Taupo Volcanic Zone, New Zealand: Its distribution and nature, *N. Z. J. Geol. Geophys.*, *42*, 533–542, doi:10.1080/00288306.1999.9514859.

Chen, C. W., and H. A. Zebker (2002), Phase unwrapping for large SAR interferograms: Statistical segmentation and generalized network models, *IEEE Trans. Geosci. Remote Sens.*, *40*, 1709–1719, doi:10.1109/TGRS.2002.802453.

Davis, P. M. (1986), Surface deformation due to inflation of an arbitrarily oriented triaxial ellipsoidal cavity in an elastic half-space, with reference to Kilauea Volcano, Hawaii, *J. Geophys. Res.*, *91*, 7429–7438, doi:10.1029/JB091iB07p07429.

Dzurisin, D., M. Lisowski, C. W. Wicks, M. P. Poland, and E. T. Endo (2006), Geodetic observations and modeling of magmatic inflation at the Three Sisters volcanic center, central Oregon Cascade Range, USA, *J. Volcanol. Geotherm. Res.*, *150*, 35–54, doi:10.1016/j.jvolgeores.2005.07.011.

Dzurisin, D., M. Lisowski, and C. W. Wicks (2009), Continuing inflation at Three Sisters volcanic center, central Oregon Cascade Range, USA, from GPS, leveling, and InSAR observations, *Bull. Volcanol.*, *71*, 1091–1110, doi:10.1007/s00445-009-0296-4.

Evans, W. C., M. C. van Soest, R. H. Mariner, S. Hurwitz, S. E. Ingebritsen, C. W. Wicks Jr., and M. E. Schmidt (2004), Magmatic intrusion west of Three Sisters, central Oregon, USA: The perspective from spring geochemistry, *Geology*, *32*, 69–72, doi:10.1130/G19974.1.

Ewert, J. W., M. Guffanti, and T. L. Murray (2005), An assessment of volcanic threat and monitoring capabilities in the United States–Framework for a National Volcanic Early Warning Systems (NVEWS), *U.S. Geol. Surv. Open File Rep.*, *2005-1164*, 62 pp.

Farr, T. G., and M. Kobrick (2000), Shuttle Radar Topography Mission produces a wealth of data. *Eos Trans. AGU*, *81*(48), 583, doi:10.1029/EO081i048p00583.

Fournier, T. J., M. E. Pritchard, and S. N. Riddick (2010), Duration, magnitude, and frequency of subaerial volcano deformation events: New results from Latin America using InSAR and a global synthesis, *Geochem. Geophys. Geosyst.*, *11*, Q01003, doi:10.1029/2009GC002558.

Galland, O., P. R. Cobbold, J. de Bremond d'Ars, and E. Hallot (2007), Rise and emplacement of magma during horizontal shortening of the brittle crust: Insights from experimental modeling, *J. Geophys. Res.*, *112*, B06402, doi:10.1029/2006JB004604.

Grandin, R., A. Socquet, M. P. Doin, E. Jacques, J. B. de Chabalier, and G. C. P. King (2010), Transient rift opening in response to multiple dike injections in the Manda Hararo rift (Afar, Ethiopia) imaged by time-dependent elastic inversion of interferometric synthetic aperture radar data, *J. Geophys. Res.*, *115*, B09403, doi:10.1029/2009JB006883.

Gudmundsson, A. (1990), Emplacement of dikes, sills and crustal magma chambers at divergent plate boundaries,

Tectonophysics, *176*, 257–275, doi:10.1016/0040-1951(90)90073-H.

Hansen, J., D. A. Jerram, K. McCaffrey, and S. R. Passey (2011), Early Cenozoic saucer-shaped sills of the Faroe Islands: An example of intrusive styles in basaltic lava piles, *J. Geol. Soc.*, *168*, 159–178, doi:10.1144/0016-76492010-012.

Hildreth, W. (2007), Quaternary magmatism in the Cascades–Geologic perspectives, *U.S. Geol. Surv. Prof. Pap.*, *1744*, 136 pp.

Hill, D. P. (1992), Temperatures at the base of the seismogenic crust beneath Long Valley caldera, California, and the Phlegrean Fields caldera, Italy, in *Volcanic Seismology*, *IAVCEI Proc. Volcanol*, vol. 3, edited by P. Gasparini et al., pp. 433–461, Springer, New York.

Hooper, A. (2008), A multi-temporal InSAR method incorporating both persistent scatterer and small baseline approaches, *Geophys. Res. Lett.*, *35*, L16302, doi:10.1029/2008GL034654.

Hooper, A., P. Segall, and H. Zebker (2007), Persistent scatterer InSAR for crustal deformation analysis, with application to Volcan Alcedo, Galapagos, *J. Geophys. Res.*, *112*, B07407, doi:10.1029/2006JB004763.

Ingebritsen, S. E., R. H. Mariner, and D. R. Sherrod (1994), Hydrothermal systems of the Cascade Range, north-central Oregon, *U.S. Geol. Surv. Prof. Pap.*, *1044-L*, 86.

Lohman, R. B., and M. Simons (2005), Some thoughts on the use of InSAR data to constrain models of surface deformation: Noise structure and data downsampling, *Geochem. Geophys. Geosyst.*, *6*, Q01007, doi:10.1029/2004GC000841.

Lu, Z., C. Wicks Jr., D. Dzurisin, J. A. Power, S. C. Moran, and W. Thatcher (2002), Magmatic inflation at a dormant stratovolcano: 1996–1998 activity at Mount Peulik volcano, Alaska, revealed by satellite radar interferometry, *J. Geophys. Res.*, *107*(B7), 2134, doi:10.1029/2001JB000471.

Lu, Z., T. Masterlark, D. Dzurisin, R. Rykhus, and C. Wicks Jr. (2003), Magma supply dynamics at Westdahl volcano, Alaska, modeled from satellite radar interferometry, *J. Geophys. Res.*, *108*(B7), 2354, doi:10.1029/2002JB002311.

Menand, T. (2011), Physical controls and depth of emplacement of igneous bodies: A review, *Tectonophysics*, *500*, 11–19, doi:10.1016/j.tecto.2009.10.016.

Menand, T., and J. C. Phillips (2007), Gas segregation in dykes and sills, *J. Volcanol. Geotherm. Res.*, *159*, 393–408, doi:10.1016/j.jvolgeores.2006.08.003.

Miller, R. G. (1974), The jackknife-a review, *Biometrika*, *61*, 1–15.

Mogi, K. (1958), Relations between the eruptions of various volcanoes and the deformations of the ground surfaces around them, *Bull. Earthquake Res. Inst. Univ. Tokyo*, *36*, 99–134.

Moran, S. C. (1994), Seismicity at Mount St. Helens, 1987–1992: Evidence for repressurization of an active magmatic system, *J. Geophys. Res.*, *99*, 4341–4354, doi:10.1029/93JB02993.

Moran, S. C. (2004), Seismic monitoring at Cascade volcanic centers, 2004—Status and recommendations, *U.S. Geol. Surv. Invest. Rep.*, *2004-5211*, 28 pp.

Newman, A. V., T. H. Dixon, G. I. Ofoegbu, and J. E. Dixon (2001), Geodetic and seismic constraints on recent activity at Long Valley Caldera, California: Evidence for viscoelastic rheology, *J. Volcanol. Geotherm. Res.*, *105*, 183–206, doi:10.1016/S0377-0273(00)00255-9.

Newman, A. V., T. H. Dixon, and N. Gourmelen (2006), A four-dimensional viscoelastic deformation model for Long Valley Caldera, California, between 1995 and 2000, *J. Volcanol. Geotherm. Res.*, *150*, 244–269, doi:10.1016/j.jvolgeores.2005.07.017.

Nichols, M. L., S. D. Malone, S. C. Moran, W. A. Thelen, and J. E. Vidale (2011), Deep long-period earthquakes beneath Washington and Oregon volcanoes, *J. Volcanol. Geotherm. Res.*, *200*, 116–128, doi:10.1016/j.jvolgeores.2010.12.005.

Pallister, J. S., R. P. Hoblitt, D. R. Crandell, and D. R. Mullineaux (1992), Mount St. Helens a decade after the 1980 eruptions: Magmatic models, chemical cycles, and a revised hazards assessment, *Bull. Volcanol.*, *54*, 126–146, doi:10.1007/BF00278003.

Pedersen, R., and F. Sigmundsson (2004), InSAR based sill model links spatially offset areas of deformation and seismicity for the 1994 unrest episode at Eyjafjallajökull volcano, Iceland, *Geophys. Res. Lett.*, *31*, L14610, doi:10.1029/2004GL020368.

Rosen, P. A., S. Henley, G. Peltzer, and M. Simons (2004), Updated repeat orbit interferometry package released, *Eos Trans. AGU*, *85*(5), 47, doi:10.1029/2004EO050004.

Ruscitto, D. M., P. J. Wallace, E. R. Johnson, A. J. R. Kent, and I. N. Bindeman (2010), Volatile contents of mafic magmas from cinder cones in the Central Oregon High Cascades: Implications for magma formation and mantle conditions in a hot arc, *Earth Planet. Sci. Lett.*, *298*, 153–161, doi:10.1016/j.epsl.2010.07.037.

Rutherford, M. J., H. Sigurdsson, S. Carey, and A. Davis (1985), The May 18, 1980, eruption of Mount St. Helens: 1. Melt composition and experimental phase equilibria, *J. Geophys. Res.*, *90*, 2929–2947, doi:10.1029/JB090iB04p02929.

Sandwell, D. T., and E. Price (1998), Phase gradient approach to stacking interferograms, *J. Geophys. Res.*, *103*, 30,183–30,204, doi:10.1029/1998JB900008.

Sandwell, D. T., D. Myer, R. Mellors, M. Shimada, B. Brooks, and J. Foster (2008), Accuracy and resolution of ALOS interferometry: Vector deformation maps of the Father's Day Intrusion at Kilauea, *IEEE Trans. Geosci. Remote Sens.*, *46*, 3524–3534, doi:10.1109/TGRS.2008.2000634.

Scandone, R., and S. D. Malone (1985), Magma supply, magma discharge and readjustment of the feeding system of Mount St. Helens during 1980, *J. Volcanol. Geotherm. Res.*, *23*, 239–262, doi:10.1016/0377-0273(85)90036-8.

Schmidt, D. A., and R. Bürgmann (2003), Time-dependent land uplift and subsidence in the Santa Clara valley, California, from a large interferometric synthetic aperture radar data set, *J. Geophys. Res.*, *108*(B9), 2416, doi:10.1029/2002JB002267.

Schmidt, M. E., and A. L. Grunder (2011), Deep mafic roots to arc volcanoes: Mafic recharge and differentiation of basaltic andesite at North Sister Volcano, Oregon Cascades, *J. Petrol.*, *52*, 603–641, doi:10.1093/petrology/egq094.

Scott, W. E., R. M. Iverson, S. P. Schilling, and B. J. Fisher (2001), Volcano hazards in the Three Sisters region, Oregon, *U.S. Geol. Surv. Open File Rep.*, *99-437*, 18.

Scott, W. E., D. R. Sherrod, and C. A. Gardner (2008), Overview of the 2004 to 2006, and Continuing, Eruption of Mount St. Helens, Washington, in *A Volcano Rekindled: The Renewed Eruption of Mount St. Helens, 2004–2006*, edited by D. R. Sherrod et al., *U.S. Geol. Surv. Prof Pap.*, *1750*, 3–22.

Sherrod, D. R., and J. G. Smith (1990), Quaternary extrusion rates of the Cascade Range, northwestern United States and southern British Columbia, *J. Geophys. Res.*, *95*, 19,465–19,474, doi:10.1029/JB095iB12p19465.

Sherrod, D. D., E. M. Taylor, M. L. Ferns, W. E. Scott, R. M. Conrey, and G. A. Smith (2004), Geologic map of the Bend

30- by 60- minute quadrangle, central Oregon, *U.S. Geol. Surv. Misc. Invest. Map*, *I-2683*, 48.

Soosalu, H., J. Key, R. S. White, C. Knox, P. Einarsson, and S. S. Jakobsdóttir (2010), Lower-crustal earthquakes caused by magma movement beneath Askja volcano on the north Iceland rift, *Bull. Volcanol.*, *72*, 55–62, doi:10.1007/s00445-009-0297-3.

Taylor, E. M. (1981), Central High Cascade roadside geology, Bend, Sisters, McKenzie Pass, and Santiam Pass, Oregon, *U.S. Geol. Surv. Circ.*, *838*, 55–58.

Valentine, G. A., and K. E. C. Krogh (2006), Emplacement of shallow dikes and sills beneath a small basaltic volcanic center—The role of pre-existing structure (Paiute Ridge, souther Nevada, USA), *Earth Planet. Sci. Lett.*, *246*, 217–230, doi:10.1016/j.epsl.2006.04.031.

White, R. S., J. Drew, H. R. Martens, J. Key, H. Soosalu, and S. S. Jakobsdóttir (2011), Dynamics of dyke intrusion in the mid-crust of Iceland, *Earth Planet. Sci. Lett.*, *304*, 300–312, doi:10.1016/j.epsl.2011.02.038.

White, S. M., J. A. Crisp, and F. J. Spera (2006), Long-term volumetric eruption rates and magma budgets, *Geochem. Geophys. Geosyst.*, *7*, Q03010, doi:10.1029/2005GC001002.

Wicks, C. W., Jr., D. Dzurisin, S. Ingebritsen, W. Thatcher, Z. Lu, and J. Iverson (2002), Magmatic activity beneath the quiescent Three Sisters volcanic center, central Oregon Cascade Range, USA, *Geophys. Res. Lett.*, *29*(7), 1122, doi:10.1029/2001GL014205.

Wicks, C., J. C. de la Llera, L. E. Lara, and J. Lowenstern (2011), The role of dyking and fault control in the rapid onset of eruption at Chaitén volcano, Chile, *Nature*, *478*, 374–377, doi:10.1038/nature10541.

Williams, C. A., and G. Wadge (2000), An accurate and efficient method for including the effects of topography in three-dimensional elastic models of ground deformation with applications to radar interferometry, *J. Geophys. Res.*, *105*(B4), 8103–8120, doi:10.1029/1999JB900307.

Williams, H. (1944), Volcanoes of the Three Sisters region, Oregon Cascades, *Univ. Calif. Pub.*, *27*, 37–84.

Yang, X., and P. M. Davis (1986), Deformation due to a rectangular tension crack in an elastic half-space, *Bull. Seismol. Soc. Am.*, *76*, 865–881.

Zebker, H. A., P. A. Rosen, and S. Hensley (1997), Atmospheric effects in interferometric synthetic aperture radar surface deformation and topographic maps, *J. Geophys. Res.*, *102*, 7547–7563, doi:10.1029/96JB03804.